



Plasma membrane association and resistosome formation of plant helper immune receptors

Zaiqing Wang^{a,1}, Xiaoxiao Liu^{a,1}, Jie Yu^a, Shuining Yin^a, Wenjuan Cai^a, Nak Hyun Kim^{b,c}, Farid El Kasmi^d, Jeffery L. Dangl^{b,c}, and Li Wan^{a,2}

Edited by Roger W. Innes, Indiana University Bloomington, Bloomington, IN; received January 5, 2023; accepted June 21, 2023 by Editorial Board Member Julian I. Schroeder

Intracellular plant immune receptors, termed NLRs (Nucleotide-binding Leucine-rich repeat Receptors), confer effector-triggered immunity. Sensor NLRs are responsible for pathogen effector recognition. Helper NLRs function downstream of sensor NLRs to transduce signaling and induce cell death and immunity. Activation of sensor NLRs that contain TIR (Toll/interleukin-1receptor) domains generates small molecules that induce an association between a downstream heterodimer signalosome of EDS1 (EnhancedDisease Susceptibility 1)/SAG101 (Senescence-AssociatedGene 101) and the helper NLR of NRG1 (NRequired Gene 1). Autoactive NRG1s oligomerize and form calcium signaling channels largely localized at the plasma membrane (PM). The molecular mechanisms of helper NLR PM association and effector-induced NRG1 oligomerization are not well characterized. We demonstrate that helper NLRs require positively charged residues in their N-terminal domains for phospholipid binding and PM association before and after activation, despite oligomerization and conformational changes that accompany activation. We demonstrate that effector activation of a TIR-containing sensor NLR induces NRG1 oligomerization at the PM and that the cytoplasmic pool of EDS1/SAG101 is critical for cell death function. EDS1/SAG101 cannot be detected in the oligomerized NRG1 resistosome, suggesting that additional unknown triggers might be required to induce the dissociation of EDS1/SAG101 from the previously described NRG1/EDS1/SAG101 heterotrimer before subsequent NRG1 oligomerization. Alternatively, the conformational changes resulting from NRG1 oligomerization abrogate the interface for EDS1/SAG101 association. Our data provide observations regarding dynamic PM association during helper NLR activation and underpin an updated model for effector-induced NRG1 resistosome formation.

plant immunity | NLR immune receptor | sensor NLR | helper NLR | cell death

Plants employ both cell surface and intracellular immune receptors to detect pathogens. Cell surface Pattern Recognition Receptors (PRRs) recognize Pathogen-Associated Molecular Patterns (PAMPs) and initiate PAMP-triggered immunity (PTI) (1). Intracellular immune receptors known as Nucleotide-binding Leucine-rich repeat Receptor (NLR) proteins recognize corresponding effectors secreted by pathogens into plant cells and initiate ETI (2). Plant NLRs express three main types of N-terminal domains: a Toll/interleukin-1 receptor, *R* genes (TIR) domain, a coiled-coil (CC) domain, or an RPW8 (Resistance to Powdery Mildew 8)-like CC (CC^R) domain. CC and CC^R domains adopt a conserved structure fold of 4-helical bundles (4HB) with the CC^R expressing an extra N-terminal region (3). TIR-NLR, CC-NLR, and CC^R-NLR are known as TNL, CNL, and RNL, respectively (4). TNL and CNL recognize pathogen effectors to trigger cell death and immune responses and are thus termed sensor NLRs. Downstream of sensor NLRs, many seed plants also deploy helper NLRs to transduce signals. There are three described classes of helper NLRs. The Activated Disease Resistance 1 (ADR1) family and the N Required Gene 1 (NRG1) family are highly conserved across the land plant phylogeny (5–7). ADR1s and NRG1s belong to the RNL family and are partially redundant downstream immune mediators of TNLs and some CNLs (8). NRCs are a greatly expanded helper NLR class in several plant families, including the Solanaceae (9). NRCs contain canonical CC domains at their N termini. In *Nicotiana benthamiana* (*Nb*), three NRCs function redundantly downstream of diverse sensor CNLs to regulate cell death and immune responses (10).

Upon effector recognition, many tested sensor CNLs and TNLs oligomerize and undergo radical conformational changes. For example, the Arabidopsis CNL AtZAR1 and wheat CNL Sr35 form pentameric resistosomes and function as Ca²⁺ permeable channels to directly induce cell death and defense responses (11–15). In contrast, activated sensor TNLs form tetrameric resistosomes that are holoenzymes cleaving NAD⁺ to produce small signaling molecules (16–22). These small molecules bind to the

Significance

Plants express diverse intracellular immune receptors that activate defense against pathogen infections. These include “sensor” NLRs (Nucleotide-binding Leucine-rich repeat Receptors) that recognize pathogen effectors and “helper” NLRs that act with unequal redundancy downstream of sensor NLRs to transduce recognition into effective immune responses. We report here that helper NLRs employ conserved positively charged residues in their N-terminal signaling domains for phospholipid binding and plasma membrane (PM) association. We demonstrate that effector-induced plant helper NLR oligomers at the PM likely only contain helper NLR molecules.

Author affiliations: ^aNational Key Laboratory of Plant Molecular Genetics, Chinese Academy of Sciences Center for Excellence in Molecular Plant Sciences, Institute of Plant Physiology and Ecology, Chinese Academy of Sciences, Shanghai 200032, China; ^bHHMI, University of North Carolina at Chapel Hill, Chapel Hill, NC 27599; ^cDepartment of Biology, University of North Carolina at Chapel Hill, Chapel Hill, NC 27599; and ^dCentre for Plant Molecular Biology (ZMBP), University of Tübingen, 72076 Tübingen, Germany

Author contributions: Z.W., X.L., J.L.D., and L.W. designed research; Z.W., X.L., J.Y., S.Y., and W.C. performed research; Z.W., X.L., J.Y., S.Y., W.C., N.H.K., F.E.K., J.L.D., and L.W. analyzed data; and J.L.D. and L.W. wrote the paper.

The authors declare no competing interest.

This article is a PNAS Direct Submission. R.W.I. is a guest editor invited by the Editorial Board.

Copyright © 2023 the Author(s). Published by PNAS. This open access article is distributed under [Creative Commons Attribution License 4.0 \(CC BY\)](https://creativecommons.org/licenses/by/4.0/).

¹Z.W. and X.L. contributed equally to this work.

²To whom correspondence may be addressed. Email: lwan@cemps.ac.cn.

This article contains supporting information online at <https://www.pnas.org/lookup/suppl/doi:10.1073/pnas.2222036120/-/DCSupplemental>.

Published July 31, 2023.

heterodimers of the Enhanced Disease Susceptibility 1 (EDS1) with either Senescence-Associated Gene 101 (SAG101) or Phytoalexin Deficient 4 (PAD4) (19, 20). In Arabidopsis, AtEDS1 and AtSAG101 form a stable heterodimer and cooperate with the AtNRG1s to mainly control cell death, while AtEDS1 and AtPAD4 physically associate and function with the AtADR1s to mainly mediate bacterial growth restriction, resistance, and transcriptional reprogramming (6, 7, 19, 20, 23, 24), although there are some overlapping functions (8). The autoactive AtNRG1 mutant and AtADR1 were demonstrated to oligomerize and function as Ca^{2+} permeable channels to induce cell death independent of the lipase-like proteins (3). It is currently unknown whether TNL activation is sufficient to trigger RNL oligomerization and whether EDS1/SAG101 and EDS1/PAD4 are present in NRG1 and ADR1 resistosomes, respectively.

Sensor NLRs are localized in their resting states to various places in the cell, likely in order to engage with the relevant appropriately localized effectors. Consistent with their proposed Ca^{2+} channel activities, some activated CNLs and RNLs exhibit PM (plasmamembrane) localization (3, 12–15, 25, 26). The Arabidopsis CNL RPM1 associates with the PM and remains at the PM after its activation by PM-targeted effectors that modify its guarder protein RIN4 (25, 27). The Arabidopsis CNL RPS5 also localizes to the PM via an N-terminal acylation signal and functions at the PM (26). By contrast, AtZAR1 distributes mainly in the cytoplasm in the resting state (13). Upon activation, AtZAR1 moves to, oligomerizes at, and presumably protrudes through the PM to form an active Ca^{2+} channel (11, 12, 28). Plant helper NLRs including ADR1s, NRG1s, and NRCs contain no predicted acylation signal but still localize at the PM before activation (3, 29, 30). AtNRG1.1 localizes to the PM, partially to endoplasmic reticulum (ER) membranes and in the cytosol when transiently overexpressed in *Nb* (3, 31). Arabidopsis ADR1s mainly localizes at the PM in a phospholipid-dependent manner since depletion of phosphatidylinositol-4-phosphate (PI4P) from the PM by overexpression of the yeast phospholipid-phosphatase Sac1p led to a mislocalization of ADR1 and loss of cell death activities (29). During activation by *Phytophthora infestans* infection, NbNRC4 accumulates at the extrahaustorial membrane (EHM) (30). When activated by sensor NLRs, NbNRC4 forms puncta mainly at the EHM and, to a lesser extent, at the PM; a constitutively autoactive NbNRC4 mutant mainly exhibits PM-associated punctate distribution, similar to autoactivated AtNRG1.1 (3, 30). Given that AtNRG1.1 CC^{R} cell death activity is also affected when coexpressed with the yeast phospholipid-phosphatase Sac1p (29) and that NbNRCs do also not possess any N-terminal acylation site or predicted transmembrane anchor, it is very likely that NRG1s and NRCs also associate with PM in a phospholipid-dependent manner. However, how exactly the three subtypes of helper NLRs interact with phospholipids is unknown.

Here, we show that the three classes of helper NLRs directly interact with phospholipids via conserved positively charged residues in the second and fourth helices of their CC^{R} or CC domain to anchor at the PM in both resting and active states, despite undergoing conformational changes accompanying activation. Consistent with the previously reported activation mimic AtNRG1.1 D485V (hereafter, AtNRG1.1 DV) (3, 31), effector activation of an upstream TNL induces AtNRG1.1 oligomerization and puncta formation at the PM. Interestingly, a cytoplasmic AtEDS1/AtSAG101 fraction is important for the AtNRG1.1 cell death function, but this heterodimer cannot be detected in the oligomerized AtNRG1.1 resistosome. These results suggest that the AtEDS1/AtSAG101/AtNRG1.1 heterotrimer induced by TNL activation represents an intermediate state before dissociation of AtEDS1/AtSAG101 and subsequent oligomerization of AtNRG1.1 or that the conformational changes resulting from

AtNRG1 oligomerization abrogate the interface for AtEDS1/AtSAG101 association.

Results

Positively Charged Residues in $\alpha 4$ of the 4HB Contribute to NRG1 and NRC Phospholipid Binding and PM Localization before and after Activation. We previously demonstrated that the AtADR1 CC^{R} domain binds to phospholipids in vitro (29), but it remained unknown which residues in AtADR1 CC^{R} were responsible for that interaction. Assuming that the ADR1 and NRG1 CC^{R} domains and potentially the NRC CC could use the same mechanism for phospholipid binding and PM association, we performed sequence alignment with ADR1s, NRG1s, and NRCs from Arabidopsis and *Nb* to identify potential conserved, positively charged residues that might bind negatively charged phospholipids. We found an absolutely conserved lysine residue corresponding to K100 in AtNRG1.1 (*SI Appendix, Fig. S1A*). This lysine residue is highly conserved in ADR1s, NRG1s, and NRCs across different plant species (Fig. 1A). We did not observe conservation of this amino acid in AtRPS5 which features an N-terminal acylation signal for PM localization, in AtRPM1 which relies largely on association with RIN4 for PM association or in AtZAR1 which mainly localizes in the cytoplasm when overexpressed in *Nb* (*SI Appendix, Fig. S1 A and B*). This observation further suggests a specific and potentially functional role for the AtNRG1.1 K100 equivalent in PM localization of helper NLRs. Lipid-strip binding assays showed that purified AtNRG1.1 CC^{R} (aa 1 to 124) protein specifically binds to phospholipids including PI4P, while K100E completely abolished phospholipid binding. We note that even 2 or 5 times more K100E protein could not restore the binding to AtNRG1.1 CC^{R} wide-type (WT) level (Fig. 1B). K100E was still active in triggering cell death in *Nb*, although this phenotype was weaker than the control, AtNRG1.1 DV (Fig. 1 C and D). Considering that positively charged residues adjacent to K100 may also contribute to phospholipid binding and function, we mutated positively charged residues close to K100 in the $\alpha 4$ helix (*SI Appendix, Fig. S1C*). A quadruple mutant K100E/R103E/K106E/K110E (hereafter, g4m) and a penta mutant R99E/K100E/R103E/K106E/K110E (hereafter, g5m) completely suppressed the cell death activity of AtNRG1.1 DV (Fig. 1 C and D). The four single mutants including R99E, R103E, K106E, and K110E showed obviously or slightly reduced binding toward phospholipids in vitro (Fig. 1E). Blue-native PAGE assays showed that K100E and g4m properly oligomerized in the context of AtNRG1.1 DV, while g5m oligomerization was hindered (Fig. 1F, also showing equal mutant accumulation on sodium dodecyl sulfate-polyacrylamide gel electrophoresis (SDS-PAGE) immunoblot). Both g4m and g5m strongly affected PM locations of both AtNRG1.1 WT and DV as demonstrated in both laser confocal microscopy (hereafter, confocal) and PM fractionation assays, while K100E had a slight effect (Fig. 2 A–D). Given that the cell death function of AtNRG1.1 DV affects protein accumulation, PM fractionation experiments on AtNRG1.1 DV were performed in the context of the previously identified loss-of function mutant ΔN16 (deletion of residues 2 to 16) (Fig. 2D) (3). In confocal assays, DV K100E and DV g4m maintained the ability to form puncta at the PM, as observed for AtNRG1.1 DV, but not DV g5m (Fig. 2 C and E and *SI Appendix, Fig. S2*), consistent with their abilities to oligomerize in blue-native PAGE assays.

The corresponding lysine residue is not conserved generally across CNLs but is conserved in helper NRCs including the NRC negative regulator NbNRCX (*SI Appendix, Fig. S1A*) (32). The conserved lysine residue in the $\alpha 4$ helix of the Arabidopsis RNLs corresponds to K84 in NbNRC4. K84E/K87E/K89E/K91E/

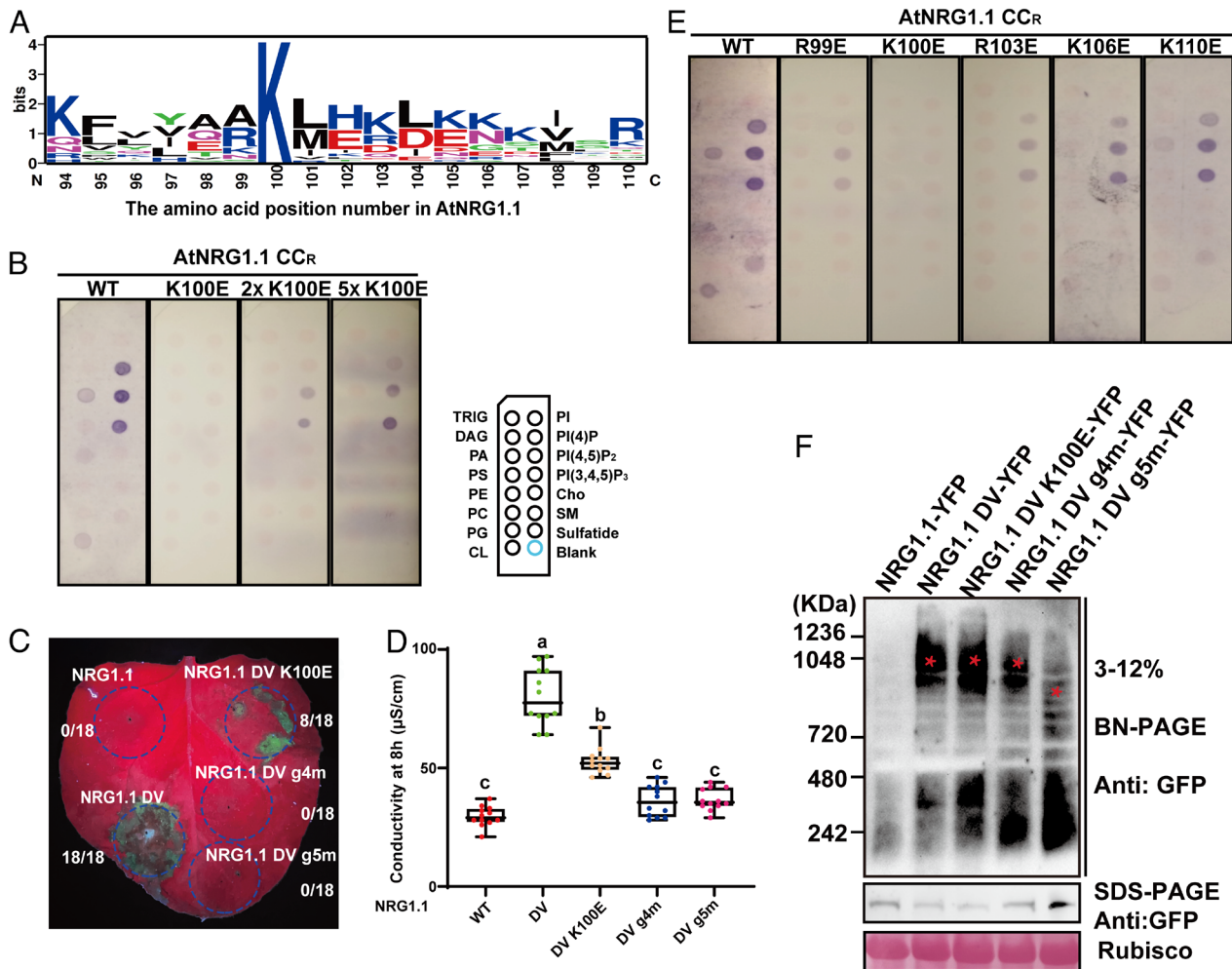


Fig. 1. Positively charged residues in the $\alpha 4$ helix of 4HB affect AtNRG1.1 CC^R phospholipid binding and AtNRG1.1 DV function. (A) Sequence logos showing the conservation of AtNRG1.1 K100 in three helper NLR families from different plant species. The alignment was performed with ClustalX, and sequence logos were generated using WEBLOGO. (B) Lipid strip binding assay using purified proteins of AtNRG1.1 CC^R (aa 1 to 124) and K100E. See *Materials and Methods* for lipid definitions. (C) Cell death phenotypes of AtNRG1.1 DV and mutants with altered PM localization in *Nb* at 32h post infiltration. (D) Quantification of ion leakage from the cell death phenotypes in C. (E) Lipid strip binding assay using purified proteins of AtNRG1.1 CC^R 1 to 124 and mutants in the $\alpha 4$ helix. (F) BN-PAGE analyses of the oligomerization of AtNRG1.1 DV mutants with altered PM localization. Red asterisks indicate oligomerized AtNRG1.1 DV or mutant derivatives.

R94E (hereafter, c5m) abolished the phospholipid binding of NbNRC4 CC in vitro (Fig. 3A) and suppressed the cell death activity of NbNRC4 D478V (hereafter, NbNRC4 DV) (Fig. 3B and C and *SI Appendix, Fig. S3A*). Moreover, c5m also attenuated the PM localization of both NbNRC4 WT (Fig. 3D and E) and NbNRC4 DV (Fig. 3F). Given the weak fluorescence signal of NbNRC4 DV due to cell death starting from 24 h post infiltration, the confocal assay on NbNRC4DV was performed in the context of the previously identified loss-of-function mutant L9E (Fig. 3F) (33). NbNRCX exhibited strong PM localization, while K84E/K89E/K92E/K93E (hereafter, x4m) exhibited reduced PM localization (Fig. 3G and H). Hence, the positively charged residues in the $\alpha 4$ helix of the 4HB contribute to NRG1 and NRC phospholipid binding and PM localization before and after activation, suggesting a conserved mechanism.

Positively Charged Residues in the $\alpha 2$ and $\alpha 4$ Helices of 4HB Collectively Affect ADR1 PM Localization before and after Activation. Mutations in the $\alpha 4$ helix of the 4HB abolished the cell death function of AtNRG1.1 DV and NbNRC4 DV, but only partially affected PM localization, indicating that additional residues may also contribute to phospholipid binding. To further investigate whether additional residues indeed contribute

to phospholipid binding, we chose to focus on AtADR1-L1 because of its distinct PM localization compared to AtNRG1.1 and NbNRC4 (29). The conserved lysine residue in the $\alpha 4$ helix corresponds to K99 in AtADR1-L1. The quadruple mutant R98, K99, K102, K105 (hereafter, r4m) in $\alpha 4$ strongly attenuated the phospholipid binding of AtADR1-L1 CC^R in vitro (Fig. 4A) and AtADR1-L1 D489V (hereafter, AtADR1-L1 DV) cell death activity (Fig. 4B and C, with protein accumulation controls in S3B). r4m affected the PM localization of both AtADR1-L1 WT (Fig. 4D and E) and AtADR1-L1 DV (Fig. 4F). Further search for conserved positively charged residues in the 4HB of RNLs identified a highly conserved K or R residue corresponding to K30 in AtADR1-L1 and K35 in AtNRG1.1 (*SI Appendix, Fig. S1A* and Fig. 4G), and the corresponding positions in NRCs are also largely conserved (*SI Appendix, Fig. S1A*). A triple mutant of K30 and adjacent positively charged residues, R28E/K30E/K34E (hereafter, r3m), reduced the phospholipid binding of AtADR1-L1 CC^R in vitro (Fig. 4A) and suppressed the cell death phenotype of AtADR1-L1 DV (Fig. 4B and C), suggesting a critical role of the positively charged residues in the $\alpha 2$ helix. Confocal and membrane fractionation assays further demonstrated that r3m affected the PM localization of both AtADR1-L1 WT (Fig. 4D and E) and DV (Fig. 4F). The combination of r3m and r4m abolished the

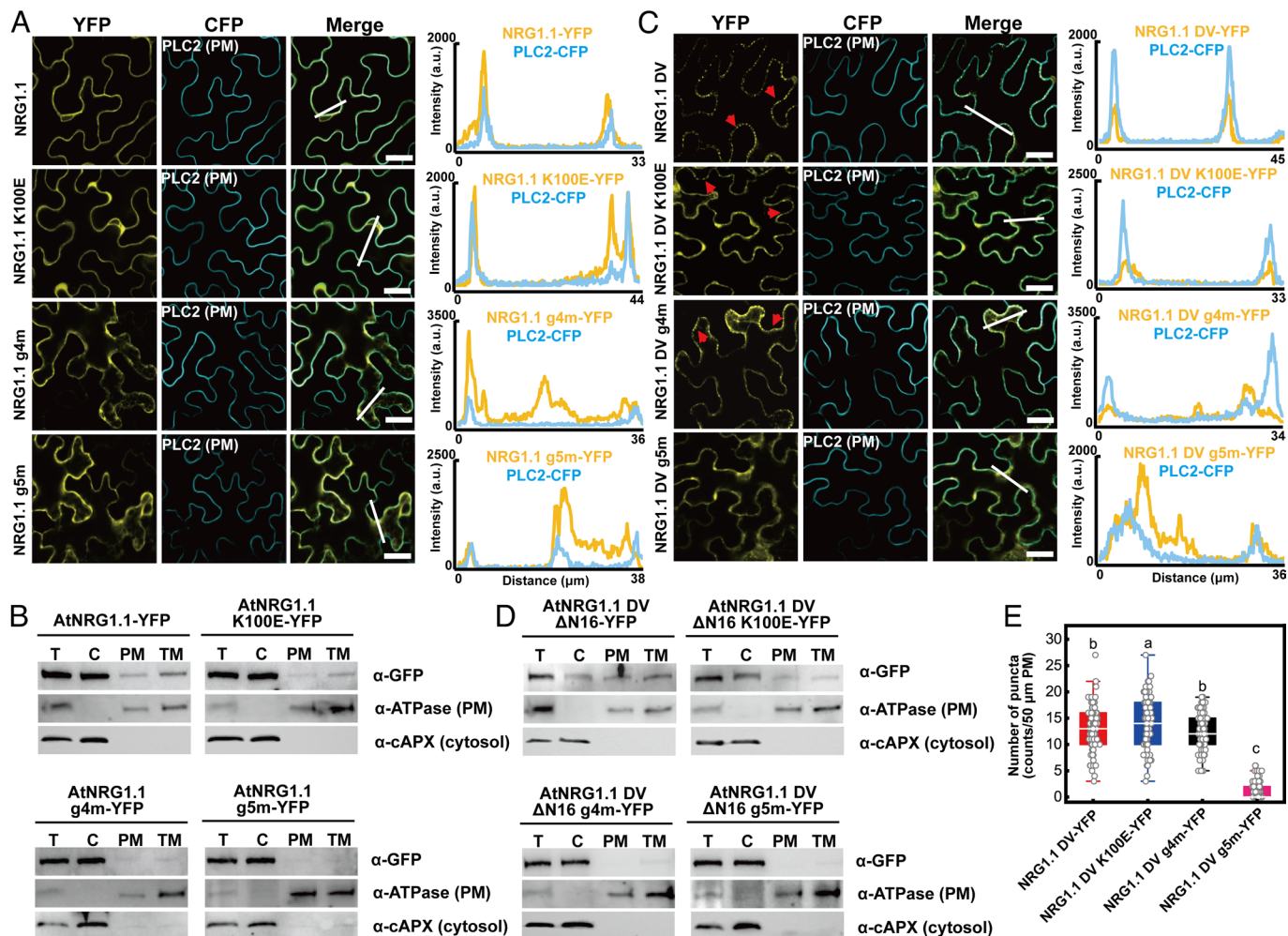


Fig. 2. Positively charged residues in the $\alpha 4$ helix of 4HB affect AtNRG1.1 and DV PM association. (A) Confocal microscopy analyses on the mutations of the positively charged residues affecting PM localization of AtNRG1.1. The indicated proteins fused with a C-terminal yellow fluorescent protein (YFP) were transiently coexpressed with the PM marker PLC2 fused to cyan fluorescent protein (CFP) in *Nb* leaves, and confocal images were taken at 32 to 36 h post infiltration. Confocal images are single plane secant views. Merge means merged image between YFP and CFP images. The red arrowheads indicated puncta. Fluorescence intensities were measured along the white line depicted in the merge images. Bars, 25 μm . (B) Membrane fractionation assays on the positively charged residues affecting AtNRG1.1 protein accumulation at the PM. (C) Confocal microscopy analyses on the mutations of the positively charged residues affecting PM localization of AtNRG1.1 DV. (D) Membrane fractionation assays on the positively charged residues affecting AtNRG1.1 DV ΔN16 protein accumulation at the PM. (E) Quantification of puncta observed in C.

phospholipid binding of AtADR1-L1 CC^R in vitro, and 2 or 5 times more r3m/r4m protein could not restore the binding to WT level (Fig. 4A). Moreover, r3m/r4m abolished the cell death activity of AtADR1-L1 DV (Fig. 4B and C) and dramatically reduced the PM localization of both AtADR1-L1 WT (Fig. 4D and E) and DV (Fig. 4F). Colocalization assays using AtVMA12 as an ER marker and RFP as a cytosolic marker indicate that the three AtADR1-L1 DV mutants localize largely in the cytosol and also at ER (SI Appendix, Fig. S3 C and D). Based on an AlphaFold structure model of AtADR1-L1 CC^R in the resting state, the two clusters of positively charged residues involved in r3m and r4m are spatially close to each other (SI Appendix, Fig. S4A). Hence, the $\alpha 2$ and $\alpha 4$ helices collectively contribute to phospholipid binding and PM localization of ADR1 before and after activation.

Our data indicate that ADR1s are localized to the PM in the resting state via the positively charged residues in the $\alpha 2$ and $\alpha 4$ helices of the 4HB that interact with phospholipids. According to the AtZAR1 activation model, the $\alpha 1$ helix flips out of the 4HB and inserts into the PM upon activation (13) (SI Appendix, Fig. S4B). The conserved positively charged residue in the $\alpha 2$ helix corresponding to K30 in AtADR1-L1 is located at the very beginning of $\alpha 2$ (SI Appendix, Fig. S2A) and could still associate with the

PM following an AtZAR1-like activation model (SI Appendix, Fig. S4B). Also, the $\alpha 4$ helix becomes disordered upon oligomerization but maintains contact with the PM (13) (SI Appendix, Fig. S4B). These conformational changes are likely to allow positively charged amino acids in the $\alpha 2$ and $\alpha 4$ helices to maintain association with the PM post activation. Hence, ADR1s rely on the conserved positively charged residues in both the $\alpha 2$ and $\alpha 4$ helices of the 4HB for phospholipid binding and PM localization before and after activation, despite the conformational changes generated by activation.

Effector Activation of a TNL Induces AtNRG1.1 Resistosome Formation at the PM. Our previous study on autoactive AtNRG1.1 DV used different loss-of-function mutations, including L134E that abolished oligomerization, ΔN16 that enhanced oligomerization, and D3N/E14Q that specifically blocked Ca²⁺ channel activity (3). It remained unknown whether AtNRG1.1 indeed oligomerizes at the PM following activation by an effector and its corresponding TNL. We transiently expressed AtEDS1/AtSAG101/AtNRG1.1 in *Nb* *epss* (*eds1a*, *pad4*, *sag101a*, and *sag101b*) leaves (6) together with the effector XopQ to reconstitute the TNL Roq1 cell death phenotype (34). AtNRG1.1 WT, but not L134E, ΔN16 , D3N/E14Q, or

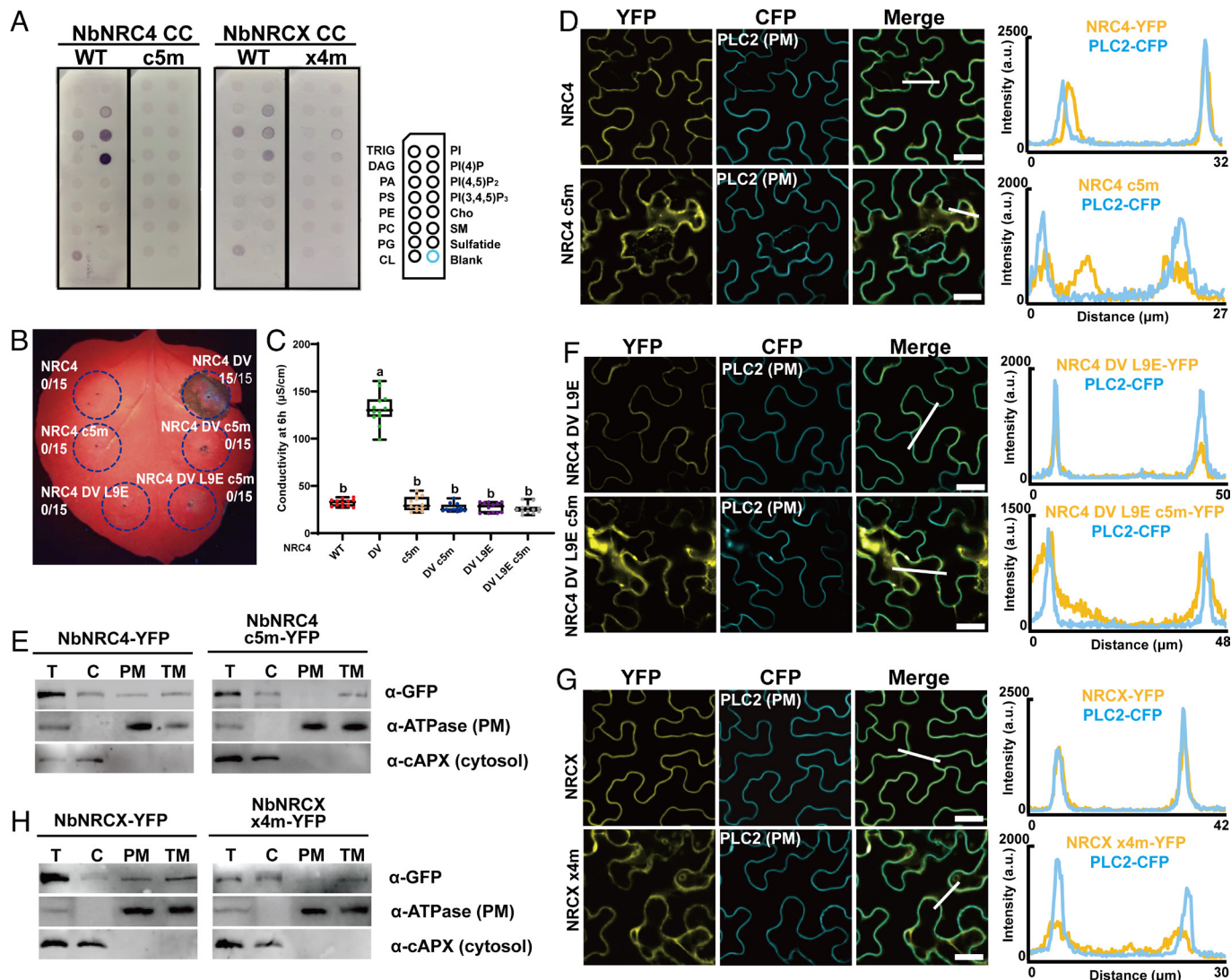


Fig. 3. Mutations of the positively charged residues in the $\alpha 4$ helix of 4HB affect NbNRC phospholipid binding, PM localization and function. (A) Lipid strip binding assay using purified proteins of NbNRC4 CC (aa 1 to 127) and its c5m mutant and NbNRCX CC (aa 1 to 129) and its x4m mutant. See *Materials and Methods* for lipid definitions. (B) Cell death phenotypes of NbNRC4 DV and mutants with altered PM localization in Nb 32 h post infiltration. (C) Quantification of ion leakage from the cell death phenotypes in B. (D) Confocal microscopy analyses on the mutations of the positively charged residues affecting PM localizations of NbNRC4. The indicated proteins fused with a C-terminal YFP were transiently coexpressed with the PM marker PLC2 fused to CFP in Nb leaves and confocal images were taken at 32 to 36 h post infiltration. Images are single plane scan views. Merge means merged images between YFP and CFP images. Fluorescence intensities were measured along the white line depicted in the merge images. Bar, 25 μ m. (E) Membrane fractionation assays on the positively charged residues affecting NbNRC4 protein accumulation at the PM. Confocal microscopy analyses on the mutations of the positively charged residues affecting PM localizations of NbNRC4 DV (F) and NbNRCX (G), respectively. (H) Membrane fractionation assays on the positively charged residues affecting NbNRCX protein accumulation at the PM.

g4m, caused cell death (Fig. 5 A and B and *SI Appendix*, Fig. S5A). We employed blue native-polyacrylamide gel electrophoresis (BN-PAGE) to investigate AtNRG1.1 oligomerization status following effector activation. AtNRG1.1 WT, Δ N16, D3N/E14Q, and g4m oligomerized following Roq1 activation by XopQ, with Δ N16 exhibiting much stronger oligomerization signal than the others; L134E failed to oligomerize (Fig. 5C). Hence, g4m specifically affects PM localization of AtNRG1.1 but not oligomerization (Figs. 1F and 2E and *SI Appendix*, Fig. S2). These cell death phenotypes and oligomerization states are consistent with the observations using the activation mimic allele AtNRG1.1 DV (Fig. 1 C, D, and F) (3). In confocal assays, AtNRG1.1 WT, D3N/E14Q, and g4m, which all maintained the ability to oligomerize, also exhibited puncta close to or on the PM, and Δ N16 displayed enhanced puncta; the loss-of-oligomerization mutant L134E exhibited no obvious puncta formation compared to AtNRG1.1 WT (Fig. 5 D–I and *SI Appendix*, Fig. S5B). These data demonstrate that effector activation of a TNL induces AtNRG1.1 resistosome formation at

the PM and that AtNRG1.1 DV faithfully mimics the functionality of effector-activated AtNRG1.1.

The Cytoplasmic Pools of AtEDS1 and AtSAG101 Mediate Cell Death but Are Not Detectable in the Oligomerized AtNRG1.1 Resistosome. AtEDS1 and AtSAG101 are localized to the nucleus and the cytoplasm (35, 36). We investigated whether enforced nuclear and cytoplasmic distribution of AtEDS1 and AtSAG101 could affect the cell death phenotype using coexpression complementation assays in *Nb eps* plants. Expression of AtEDS1 and AtSAG101 with a nuclear export signal (NES) slightly attenuated XopQ-TNL Roq1-dependent cell death comparable to wild-type AtEDS1 and AtSAG101 (Fig. 6 A and B and *SI Appendix*, Fig. S6), which agrees to some extent with previous finding showing that coexpression of NES-tagged Solanaceae EDS1 with Solanaceae SAG101 blocks XopQ triggered cell death function in *Nb eps* (37). By contrast, AtEDS1 and AtSAG101 with a nuclear localization signal (NLS) did not support cell death in this assay (Fig. 6 A and

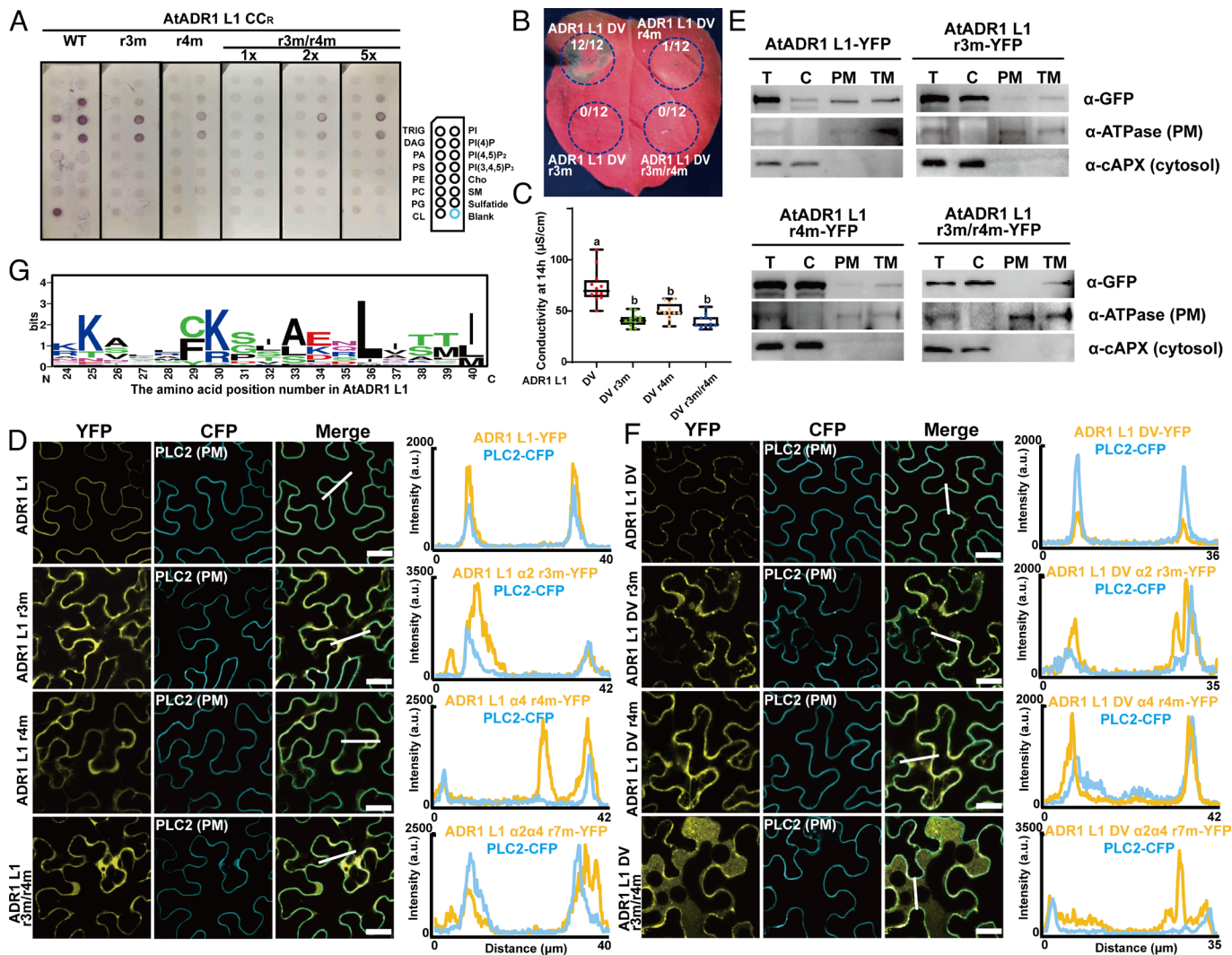


Fig. 4. Positively charged residues in the $\alpha 2$ and $\alpha 4$ helices of the 4HB collectively contribute to AtADR1-L1 phospholipid binding, PM localization and function. (A) Lipid strip binding assay using purified proteins of AtADR1-L1 CC^R (aa 1 to 114) and mutant derivatives r3m, r4m and r3m/r4m. See Materials and Methods for lipid definitions. (B) Cell death phenotypes of AtADR1-L1 DV and mutants with altered PM localization in Nb 32 h post infiltration. (C) Quantification of ion leakage from the cell death phenotypes in B. (D) Confocal microscopy analyses of the mutations of the positively charged residues affecting PM localizations of AtADR1-L1. The indicated proteins fused with a C-terminal YFP were transiently coexpressed with the PM marker PLC2 fused to CFP in Nb leaves, and confocal images were taken at 32 to 36 h post infiltration. Confocal images are single plane secant views. Merge means merged image between YFP and CFP images. Fluorescence intensities were measured along the white line depicted in the merge images. Bars, 25 μ m. (E) Membrane fractionation assays on the positively charged residues affecting AtADR1-L1 protein accumulation at the PM. (F) Confocal microscopy analyses of the mutations of the positively charged residues affecting PM localizations of AtADR1-L1 DV. (G) Sequence logos showing the conservation of AtADR1-L1 K30 in RNLs from different plant species. The alignment was performed with ClustalX, and sequence logos were generated using WEBLOGO.

B and *SI Appendix*, Fig. S6). These data suggest that the cytoplasmic pools of AtEDS1 and AtSAG101 activate AtNRG1.1 and are critical determinants of XopQ-activated cell death responses, which is consistent with a recent study showing that different TIR domains preferentially signal cell death via the cytosolic pool of EDS1 in Arabidopsis (38). Given that TIR-dependent signals induce the formation of AtEDS1/AtSAG101/AtNRG1 heterotrimers (20), we performed BN-PAGE to further investigate whether AtEDS1 and AtSAG101 are subsequently retained in the oligomerized AtNRG1.1 resistosome. AtNRG1.1 Δ N16 oligomerized in a XopQ-dependent manner following activation of the Roq1 TNL when coexpressed with AtEDS1 and AtSAG101, while AtNRG1.1 Δ N16/L134E was not responsive to XopQ (Fig. 6C and *SI Appendix*, Fig. S7). However, in samples expressing AtNRG1.1 Δ N16, with or without XopQ, or AtNRG1.1 Δ N16/L134E plus XopQ, we did not detect oligomerization of AtEDS1 (Fig. 6C, StrepII immunoblot) or AtSAG101 (Fig. 6C, Flag immunoblot) at the high-molecular-weight regions corresponding to AtNRG1.1

oligomers. We ruled out the tag effect for the negative results by detecting oligomerization of AtNRG1.1 Δ N16 with the same epitope tag as either AtEDS1 or AtSAG101 in a single gel at three different time points 26 h, 32 h, and 42 h post infiltration (Fig. 6C and *SI Appendix*, Fig. S7). Hence, AtEDS1 and AtSAG101 could not be detected in the oligomerized AtNRG1.1 resistosome in this cell death reconstitution assay in *Nb eps*. One hypothesis is that additional signals may be required to trigger the dissociation of AtEDS1/AtSAG101 and subsequent oligomerization of AtNRG1.1 after TIR-induced AtEDS1/AtSAG101/AtNRG1.1 heterotrimer formation (Fig. 6D).

Discussion

PM localization was required for Ca²⁺ channel formation or immune function of RNLs and many CNLs (3, 12, 14, 15, 25, 26, 29, 30). Helper NLRs, including NRG1s and ADR1s, exhibited significant PM location before activation (or the EHM in the

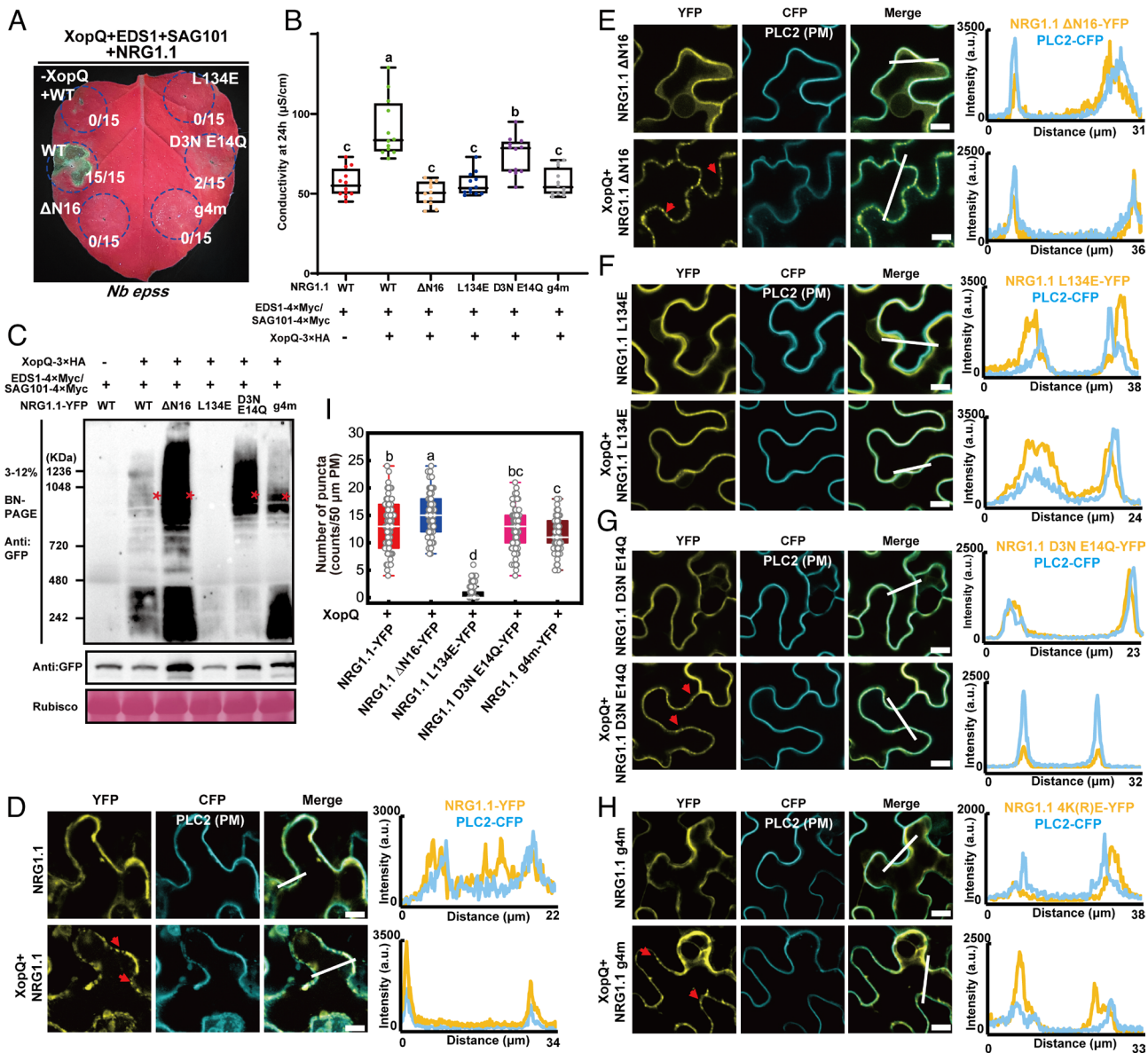


Fig. 5. Effector-induced AtNRG1.1 oligomerization and enhanced puncta formation at the PM. (A) XopQ-triggered cell death phenotypes in *Nb epss* when coexpressed with AtEDS1, AtSAG101, and AtNRG1.1 mutants 48 h post infiltration. (B) Quantification of ion leakage from the cell death phenotypes in A. (C) BN-PAGE showing the oligomerization status of AtNRG1.1 mutants in A. Red asterisks indicate oligomerized AtNRG1.1. Confocal microscopy assays showing PM localization and puncta of AtNRG1.1 (D), derivative alleles ΔN16 (E), L134E (F), D3N/E14Q (G), and g4m (H) before and postactivation via XopQ expression when coexpressed with AtEDS1 and AtSAG101. The indicated proteins fused with a C-terminal YFP were transiently coexpressed with the PM marker PLC2 fused to CFP in *Nb* leaves and confocal images were taken at 32 to 36 h post infiltration. Confocal images are single plane secant views. Merge means merged images between YFP and CFP images. The red arrowheads indicated puncta. Fluorescent intensities were measured along the white line depicted in the merge images. Bar, 10 μm. (I) Quantification of puncta as observed in D–H.

case of NbNRC4) and are further enriched and concentrated at the PM after activation (3, 29–31). Mechanisms driving helper NLR PM localization remained largely unclear.

In plants, PI4P is the main driver of PM electrostatics (39, 40). Phosphatidic acid (PA) and phosphatidylserine (PS) and PI(4, 5) P₂ [PI(4, 5)-bisphosphate] also contribute to PM (inner leaflet) surface charges, but to a lesser extent. We generated mutations in the conserved positively charged residues in the α2 and α4 helices of helper NLR 4HBs. These mutations attenuated phospholipid binding in vitro and PM association in vivo; they also abolished cell death function. Another 4HB-containing membrane pore-forming protein, the animal mixed lineage kinase domain-like, specifically interacts with phospholipids for PM localization and function (41). A recent study showed that *Mycobacterium tuberculosis* inhibits pyroptosis by secreting a phospholipid phosphatase that localizes at

the host PM to dephosphorylate PI4P and PI(4, 5)P₂ and suppresses the PM association and pore function of activated Gasdermin D (42). Hence, phospholipid-binding mediated PM association is a conserved mechanism for membrane pore-forming proteins. It remains to be investigated whether plant pathogens employ similar phospholipid phosphatases to perturb the PM localization and thus the function of helper NLRs.

We provide mechanistic insights into the dynamics of PM association during plant helper NLR activation. In the absence of pathogen infection, interactions of the α2 and α4 helices of the N-terminal 4HB anchor a significant fraction of plant helper NLRs at the PM. Upon activation by sensor NLRs, helper NLRs undergo dramatic conformational changes and further concentration at the PM; they still rely on the α2 and α4 helices to associate with the PM for function (Fig. 5C).

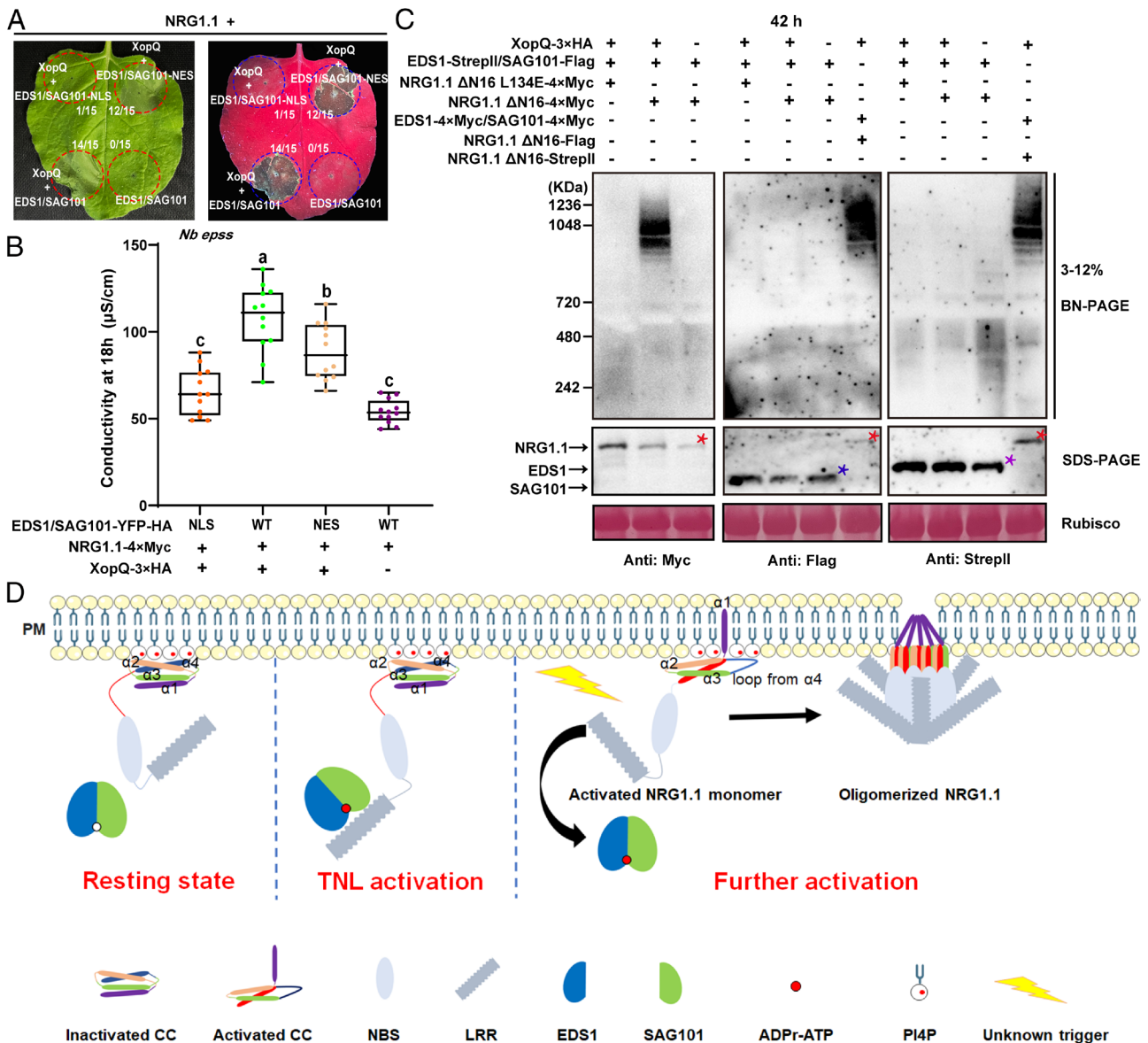


Fig. 6. AtEDS1 and AtSAG101 cannot be detected in the oligomerized AtNRG1.1 resistosome. (A) The cytoplasmic pool of EDS1/SAG101 activates NRG1.1 to induce cell death. EDS1/SAG101-NLS, EDS1/SAG101-NES, or EDS1/SAG101 with a C-terminal YFP-HA tag were transiently coexpressed with NRG1.1-4×Myc and XopQ-4×Myc in *Nb epss*. Cell death phenotypes were photographed 42 h post infiltration. (B) Quantification of ion leakage from the cell death phenotypes in A. (C) EDS1/SAG101 do not comigrate with NRG1.1 upon XopQ activation in BN-PAGE assays. *Agrobacteria* mixes carrying the indicated expression constructs were coinfiltrated into *Nb epss*. Total protein extracts were resolved by BN-PAGE and SDS-PAGE 42 h post infiltration. Target bands were immunoblotted with appropriate antibodies. The red asterisk indicates the protein band of NRG1.1. Purple and blue asterisks indicate EDS1 and SAG101 bands, respectively. (D) An updated model on PM association and effector-induced oligomerization of NRG1.

The RNL helper ADR1s and NRG1s contain an RPW8-like CC^R domain at their N termini. In addition to the 4HB, the CC^R domain has an extra N-terminal region that was previously predicted to be responsible for CC^R membrane targeting (43). Deletion of the extra N-terminal region did not affect PM localization of the activation mimic allele AtNRG1.1 DV (3) or effector-activated AtNRG1.1 (Fig. 5 D and E). Mutation of the positively charged residues in the α4 helix affected PM localization of AtNRG1.1 WT and the DV allele (Fig. 1 D and E). Despite the absolute conservation of AtNRG1.1 K100 in the CC^R domain of ADR1s and NRG1s, it is not conserved in RPW8 (SI Appendix, Fig. S14), indicating a different PM association mechanism for RPW8.

AtNRG1.1 K100 is highly conserved in RNL and NRC helpers but is less well conserved in sensor CNLs (SI Appendix, Fig. S14).

In contrast to RNL helpers, the well-studied sensor CNL AtZAR1 that also functions as a PM-localized Ca²⁺ channel post activation localizes mainly in the cytoplasm before activation (SI Appendix, Fig. S1B) (12, 13). In contrast, the sensor CNL AtRPM1 interacts with the PM-localized guarder RIN4, localizes to and signals from the PM (25, 44, 45); the sensor CNL AtRPS5 localizes to the PM via N-terminal acylation signal and functions at the PM (26). Thus, sensor NLRs express variable resting state subcellular distributions, likely reflecting the subcellular localization of the pathogen effectors they detect. Hence, helper NLRs use a specific mechanism for enrichment at the PM before activation, which may be critical for rapid calcium signal induction upon activation of ETI. It remains to be determined whether other CNLs also use similar phospholipid binding mechanisms to determine or enhance PM localization.

PTI and ETI function cooperatively and potentiate each other (46, 47), but the mechanisms that interconnect PTI and ETI remain unclear. The EDS1/PAD4/ADR1 module associates with some PM-located PRRs and is required for PTI (48–50). NbNRC3 mediates the hypersensitive cell death caused by the cell-surface receptor Cf-4 recognizing the apoplastic fungal effector Avr4 (51). An enriched or constitutive PM-bound pool of helper NLRs are potentially important for their efficient activation by PTI signals and the cooperative function between PTI and ETI. We demonstrated that NbNRCX, a negative regulator of NbNRC2 and NbNRC3 (32), also uses the conserved positively charged residues in the $\alpha 4$ helix of 4HB for PM association (Fig. 2D). We propose that the PM location of NbNRCX is important for its negative regulation of activated NbNRC2 and NbNRC3 at the PM, perhaps via the formation of mixed and thus “poisoned” oligomers.

Effector activation of sensor CNL triggers helper NRC oligomerization, and sensor CNLs are not present in the NRC oligomer complex (52, 53). We present data that ETI activated via the effector XopQ and the TNL Roq1 induces RNL AtNRG1.1 oligomerization and puncta formation at the PM (Fig. 4). A recent study showed that in Arabidopsis, the oligomerization of AtNRG1.2 requires not only effector-mediated activation of a TNL but also activation of PTI (54). Our data show that the cytoplasmic pool of AtEDS1/AtSAG101 mediates the cell death response, but that neither is readily detectable in the effector-induced oligomerized AtNRG1.1 resistosome (Fig. 5A and B). This is in contrast to the recent observation of NRG1.2/EDS1/SAG101 hetero-oligomers that were detectable only after immunoprecipitation of NRG1.2 (54). The combined data suggest that additional unknown triggers may be required to induce AtEDS1/AtSAG101 dissociation from the AtNRG1.1/AtEDS1/AtSAG101 heterotrimer and subsequent AtNRG1.1 oligomerization at the PM (Fig. 6D) or that the conformational changes resulting from oligomerization abrogate the interface(s) required for AtEDS1/AtSAG101 coassociation. It is also possible that NRG1/EDS1/SAG101 hetero-oligomers are transient, while we detected a latter stage of the oligomerized NRG1 resistosome after EDS1/SAG101 disassociate. The putative role of PTI in facilitating either the rare NRG1.2/EDS1/SAG101 hetero-oligomers or oligomeric NRG1 resistosome formation at the PM requires future investigation.

Materials and Methods

Plant Growth Conditions. *Nb* WT and *Nb* *epss* plants were grown in a growth chamber at 25 °C under a 16 h/8 h light/dark cycle with relative humidity at 55 ± 10%.

Vector Construction. The coding sequences (CDSs) of *AtNRG1.1* (At5g66900), *AtEDS1* (At3g48090), *AtSAG101* (At5g14930), and *AtADR1-L1* (At4g33300) were amplified using specific primers from the Arabidopsis ecotype Col-0, and the CDSs of *NbNRC4* (NbS00016103g0004, 2,464 bp) and *NbNRCX* (NbS00030243g0001, 2,619 bp) were amplified by PCR from *Nb*. The resulting PCR fragments were cloned into a modified pUC19 vector with the gateway-compatible recombination sites (attL1/attL2). The StrepII tag sequence was fused to the 3' cDNA of *AtEDS1* to obtain an *AtEDS1-StrepII* entry clone. *AtNRG1.1Δ16* was PCR-amplified using the CDS of *AtNRG1.1* as a template and then cloned into the entry vector pUC19. Other *AtNRG1.1* variants were generated using the Fast Mutagenesis System protocol (Transgene). *XopQ* with attL1/attL2 sequences was synthesized into a pUC18 plasmid (GenScript). *XopQ* was introduced to expression vectors pGWB614 and pGWB617 to obtain 35S::*XopQ-3×HA* and 35S::*XopQ-4×Myc* constructs, respectively. *AtEDS1* and *AtEDS1-StrepII* were recombined into pGWB617 (35S promoter, C-terminal 3×Myc) and pGWB2 (35S promoter, no tag), respectively. *AtSAG101* was introduced to pGWB11 (35S promoter, C-terminal Flag) and pGWB617. *AtNRG1.1* and the mutants were introduced into pGWB641 (35S promoter, C-terminal EYFP), pGWB617,

the modified vectors pEarlyGate-Flag (35S promoter, C-terminal Flag) and pEarlyGate-StrepII (35S promoter, C-terminal StrepII) to express fusion proteins with desired tags. All target sequences were introduced into expression vectors using LR reactions (Life Technologies). 35S::*AtEDS1-YFP-HA-NLS* (or *NES*) and 35S::*AtSAG101-YFP-HA-NLS* (or *NES*) expression constructs were obtained using LR to recombine pUC19-*AtEDS1*, pUC19-*AtSAG101* with modified vectors pEarlyGate 101-NLS and pEarlyGate 101-NES (55). *NbNRC4* and *NbNRCX* and their mutants were introduced into the 35S-omega-driven destination vector pEarlyGate with a C-terminal YFP-HA. The CDSs of PM marker *PLC2* (*At3g08510*) and endoplasmic reticulum marker *VMA12* (*At5g52980*) were amplified from Col-0 and subsequently cloned into PUC19/Kan vector including attR1/attR2 sites. *PLC2-CFP* expression vector and *VMA12-RFP* were generated by Golden Gate assembly with 35S-driven pEarly101 with a C-terminal CFP and 35S-driven pGWB257 with a C-terminal RFP, respectively. The obtained expression constructs were transformed into *Agrobacterium tumefaciens* GV3101 via electroporation for transient expression in *Nb*.

Transient Expression in *Nb*. *Agrobacterium* (GV3101) carrying the constructs were grown overnight in Luria Bertani medium (LB) with suitable antibiotics. Three milliliters of *Agrobacterium* culture was centrifuged and resuspended in MES buffer (10 mM MgCl₂, 10 mM MES pH 5.6, and 150 μM acetosyringone). *Agrobacterium* were incubated at room temperature for 1 h and infiltrated into the leaves of 5-wk-old *Nb* or *Nb* *epss* at specific OD₆₀₀ values. *Agrobacterium* containing the *P19* construct were coinfiltrated at an OD₆₀₀ of 0.1. Cell death phenotypes were photographed at indicated time point.

Ion Leakage Assays. Four leaf disks 8 mm in diameter were harvested 24 h after transient expression in *Nb* leaves. Leaf disks were washed for 1 h in 10 mL ultrapure water and transferred into 15-mL tubes containing 6 mL ultrapure water. Conductivity was measured using a conductivity meter (FiveGo Cond meter F3, METTLER TOLEDO) at the indicated time point. Three biological repeats and 4 technical repeats were performed. Statistical analysis was performed via Tukey's Honestly Significant Difference using GraphPad Prism 8. Different letters indicate statistically significant differences.

Total Protein Extraction and Western Blot Analysis. Three 8-mm leaf disks were harvested and ground to powder in liquid nitrogen. Total protein was extracted with 100 μL extraction buffer (20 mM Tris-HCl pH 8.0, 5 mM ethylene diamine tetraacetic acid (EDTA), 1% SDS, and 10 mM DL-dithiothreitol (DTT)). Lysate was boiled at 95 °C with 1× protein loading buffer for 10 min. The total protein extract was cleared by centrifuge at 13,000 g for 10 min. Then, the supernatant was separated by 10% SDS-PAGE gels and detected with corresponding antibodies. Antibodies used for immunoblotting include anti-GFP (#G1544, Sigma), anti-HA (#11867423001, Roche), anti-Myc (#M4439, Sigma), anti-Flag (#SAB4301135, Sigma), anti-StrepII (#ab76949, Abcam), and HRP-conjugated antibodies (#IMR-GtxMu-003-DHRPX, #IMR-GtxRb-003-DHRPX, and #GtxRt-003-DHRPX, Jackson).

BN-PAGE. BN-PAGE was performed as previously described with slight modifications (3). Three leaf disks (5 mm diameter) were homogenized with liquid nitrogen. 1× NativePAGE™ Sample Buffer (BN2008, Invitrogen™) with 1× protease inhibitor cocktail was added to the homogenized samples. The mixed samples were centrifuged at 20,000 g for 30 min at 4°C. Native PAGE™ 5% G-250 Sample Additive (BN2004, Invitrogen™) was added to the supernatant at a final concentration of 0.125%. Proteins were separated by Native PAGE™ Novex® 3 to 12% Bis-Tris Gels (BN1001, Invitrogen™) and transferred to polyvinylidene fluoride (PVDF) membrane using an eBlot™ L1 transfer system (GenScript). The target proteins were probed with corresponding antibodies.

Confocal Microscopy Analyses. For *Agrobacterium*-mediated transient expression in *Nb*, OD₆₀₀ cultures were adjusted to 0.1 of P19, 0.2 of PM or ER marker (PLC2-CFP, VMA12-RFP or RFP), and 0.2 of AtNRG1.1, AtADR1-L1, NbNRC4, or NbNRCX. *Agrobacterium* mixtures were infiltrated into young leaves of 4 to 6-wk-old *Nb* plants. For transient expression in *Nb* *epss*, the OD₆₀₀ was adjusted to 0.1 of P19, 0.1 of AtEDS1 and AtSAG101, and 0.2 of AtNRG1.1 and PLC2, and 0.001 for XopQ. *Agrobacterium* mixtures were infiltrated into young leaves of 4 to 6-wk-old *Nb* *epss* plants. Leaves were imaged for protein localization analyses between 36 h and 48 h post infiltration. Confocal images were taken on a confocal laser

scanning microscope LSM880 from Zeiss (Oberkochen, Germany) using the ZENblack software, via a Zeiss-C-Apochromat 20×/0.8 A20650-9901 objective or a Zeiss-W-Plan-Apochromat 421462-9900 objective. YFP was excited using a 514-nm laser, and the emission spectrum was between 516 and 556 nm; CFP was excited with a 458-nm laser, and the emission spectrum was between 463 and 513 nm; RFP was excited with a 532-nm laser, and the emission spectrum was between 570 and 620 nm. Focal plane images were processed with the ZEN blue software (Zeiss) for adjustment of brightness and contrast. The number of puncta per 50 μm PM was counted via ImageJ from 90 independent observations based on 9–12 images. Statistical analysis was performed with Turkey's Honestly Significant Difference, and different letters indicate statistically significant differences.

Membrane Fractionation Assays. PM protein isolation was carried out by slightly modifying a previously described protocol (3). In brief, sucrose buffer [20mM Tris (pH 8.0), 0.33 M sucrose, 1 mM EDTA, 5 mM DTT, and 1× Sigma plant protease inhibitor cocktail] was added to the homogenized tissue at a ratio of 5 μL per mg (FW) tissue. The extract was centrifuged at 2,000 × g for 5 min at 4 °C; then, the supernatant was transferred to a new tube and designated as total protein (T). Cytoplasmic fraction (C) was prepared by harvesting the supernatant after spinning the total protein fraction at 20,000 × g for 1 h at 4 °C. The total membrane fraction was prepared from the resulting pellet by resuspending in 200 μL of buffer B (Minute™ PM protein isolation kit, Invent Biotechnologies). After centrifugation at 7,800 × g for 15 min at 4 °C, the supernatant was transferred to 2 mL Eppendorf tube and mixed with 1.6 mL cold phosphate balanced solution (PBS) buffer mixed by vortexing and spun at 16,000 × g for 1 h at 4 °C to pellet the PM fraction. The pellet was resuspended with sucrose buffer in 4 times less volume than the soluble fraction. The resulting fraction was labeled as the PM-enriched/microsomal fraction. Proteins fractions were run on SDS-PAGE gels and analyzed by western blotting.

Sequence Alignment of Helper NLR Homologs. AtNRG1.1 and AtNRG1.2 (At5g66910.1) were used to identify NRG1 homologs in the predicted protein databases including Solanaceae Genomics Network (SGN) and Integrated Microbial Genomes. Similarly, AtADR1 (At1g33560.1), AtADRL1-L1, and AtADRL1-L2 (At5g04720.1) were used to identify ADR1 homologs. NbNRC2 (NbS00018282g0019.1 and NbS00026706g0016.1), NbNRC3 (NbS00011087g0003.1), NbNRC4 (NbS0000-2971g0007.1 and NbS00016103g0004.1), and NbNRCX (NbS00030243g0001.1) were used to identify NRC-helper clade homologs in the SGN database. Top hits from BLASTP search results in different plant species were collected for further analyses. Homologs with protein sequence identity of more than 50% were aligned in their CC or CC^R domains by CLUSTALW. The gene ID of homologs used in the alignment was listed in *SI Appendix, Table S1*.

Sequence Logos Visualization. Sequence logos of the identified conserved amino acid site in the CC or CC^R domain of helper NLRs were generated by the online software WEBLOGO (<http://weblogo.berkeley.edu/logo.cgi>) (56).

Protein Expression and Lipid-Strip Binding Assays. Sequences of AtNRG1.1 CC 1 to 124 (WT, R99E, K100E, R103E, K106E, and K110E) were subcloned into the pET24a plasmid with a N-terminal 6×His and a C-terminal StrepII tag. Proteins were expressed in *E. coli* BL21 (DE3) cells using the autoinduction method (57). Cell pellets were resuspended and lysed in buffer containing 50 mM 4-(2-hydroxyethyl) piperazine-1-ethanesulfonic acid (HEPES) (pH 8.0), 300 mM NaCl, 2 mM DTT, and

1 mM PMSF. After sonication and centrifugation at 20,000 g for 60 min, the supernatant was loaded onto a nickel HisTrap 5 mL column (GE HealthCare) pre-equilibrated with 20 mL of the wash buffer (50 mM HEPES pH 8.0, 300 mM NaCl, and 30 mM imidazole) at a 3 mL/min rate. The bound proteins were eluted with elution buffer (50 mM HEPES pH 7.5, 300 mM NaCl, and 500 mM imidazole) and further purified using size exclusion chromatography (Superdex 200 HiLoad 16/600 column) pre-equilibrated with the buffer containing 10 mM HEPES (pH 7.5), 150 mM NaCl, and 1 mM DTT. The peak fractions were confirmed by SDS-PAGE and pooled for lipid-strip binding assays.

Proteins of AtADR1 L1 CC^R 1 to 114 (WT, r3m, r4m, and r3m/r4m), NbNRC4 CC 1 to 127 (WT and c5m), and NbNRCX CC 1 to 129 (WT and x4m) were expressed and purified in the human embryonic kidney cell line 293F. The corresponding cDNAs of these constructs were subcloned into the pMink vector with an N-terminal protein A and SUMOstar tag and a C-terminal Flag tag. Plasmids were transfected into 293F cells using the polyethyleneimine method (58). Cells were grown in Union-293 Chemically Defined Medium (Union Bio) and were routinely maintained at the exponential phase in 1,000-mL shaker flasks. The flasks were agitated at 130 rpm at 37 °C in a humidified condition containing 5% CO₂. Cells were pelleted at 8,000 × g at 4 °C for 5 min using centrifugation at 72 h after transfection. Pellets were resuspended and lysed in lysis buffer (50 mM Tris-HCl, 300 mM NaCl, 0.5 mM EDTA, 10% (v/v) glycerol, 2 mM DTT, 1 mM PMSF, 5 mM ATP, 2 mM MgSO₄, 1% (v/v) cocktail, 0.9% (m/v) DNase I, and 0.2% (m/v) CHAPS, pH 7.5). After vibration at 4 °C for 60 min and centrifugation at 20,000 × g for 60 min, the supernatant was loaded onto 6 mL immunoaffinity chromatography column with 1 mL IgG beads (Smart-Life Sciences) pre-equilibrated with 50 mL of the wash buffer [50 mM Tris-HCl, 300 mM NaCl, 0.5 mM EDTA, and 10% (v/v) glycerol, pH 7.5]. The bound proteins were digested by ULPI enzyme, and further, the flow-through containing approved proteins were collected and concentrated for lipid-strip binding assays.

Lipid-strip binding assays were performed according to the manufacturer's instructions (Echelon Biosciences, Salt Lake City, UT, USA). Briefly, the PIP-strip membranes were blocked overnight at 4 °C in blocking buffer containing 0.1% Tween-20 and 4% fatty acid-free bovine serum albumin in PBS buffer. Purified proteins (0.5 μg/mL, final concentration) were incubated with the PIP-strip membranes for 1 h at room temperature and then washed three times using wash buffer containing 0.1% Tween-20 in PBS buffer. Bound proteins were detected by immunodetection of StrepII or Flag. Lipids in the strip include PI (4)-phosphate, [PI(4, 5)P₂], PI (3, 4, 5)-trisphosphate, triglyceride, diacylglycerol, PA, PS, phosphatidylethanolamine, phosphatidylcholine, phosphatidylglycerol, cardiolipin, PI, cholesterol, sphingomyelin, and 3-sulfogalactosylceramide.

Data, Materials, and Software Availability. All study data are included in the article and/or *SI Appendix*.

ACKNOWLEDGMENTS. We thank the confocal microscopy facility at CAS Ecology/Center for Excellence in Molecular Plant Sciences for technical supports. We thank Professor Jane Parker for providing *Nb eps* seeds. L.W. was supported by the National Key Laboratory of Plant Molecular Genetics, Institute of Plant Physiology and Ecology/Center for Excellence in Molecular Plant Sciences, and CAS Strategic Priority Research Program (Type-B; Project number: XDB27040214). X.L. was supported by a Postdoc Grant (Project number: 2021M693172) from the National Natural Science Foundation of China. F.E. is supported by the German Research Foundation (DFG Grants CRC1101 D09 and EL734/3-1). J.L.D. is supported by the NSF (Grant IOS-1758400) and HHMI (Howard Hughes Medical Institute). J.L.D. is a HHMI Investigator.

1. T. A. DeFalco, C. Zipfel, Review molecular mechanisms of early plant pattern-triggered immune signaling. *Mol. Cell* **81**, 3449–3467 (2021).
2. J. D. Jones, R. E. Vance, J. L. Dangl, Intracellular innate immune surveillance devices in plants and animals. *Science* **354**, aaf6395 (2016).
3. P. Jacob *et al.*, Plant “helper” immune receptors are Ca²⁺-permeable nonselective cation channels. *Science* **373**, 420–425 (2021).
4. L. M. Jubic, S. Saile, O. J. Furzer, F. El Kasmi, J. L. Dangl, Help wanted: Helper NLRs and plant immune responses. *Curr. Opin. Plant Biol.* **50**, 82–94 (2019).
5. X. X. Liu, L. Wan, Molecular insights into the biochemical functions and signalling mechanisms of plant NLRs. *Mol. Plant Pathol.* **23**, 772–780 (2022).
6. D. Lapin *et al.*, A coevolved EDS1-SAG101-NRG1 Module mediates cell death signaling by TIR-domain immune receptors. *Plant Cell* **31**, 2430–2455 (2019).
7. J. Gantner, J. Ordon, C. Kretschmer, R. Guerois, J. Stuttmann, An EDS1-SAG101 complex is essential for TNL-mediated immunity in *Nicotiana benthamiana*. *Plant Cell* **31**, 2456–2474 (2019).
8. S. C. Saile *et al.*, Two unequally redundant “helper” immune receptor families mediate *Arabidopsis thaliana* intracellular “sensor” immune receptor functions. *PLoS Biol.* **18**, e3000783 (2020).
9. H. Adachi, L. Derevnina, S. Kamoun, NLR singletons, pairs, and networks: Evolution, assembly, and regulation of the intracellular immunoreceptor circuitry of plants. *Curr. Opin. Plant Biol.* **50**, 121–131 (2019).
10. C. H. Wu *et al.*, NLR network mediates immunity to diverse plant pathogens. *Proc. Natl. Acad. Sci. U.S.A.* **114**, 8113–8118 (2017).
11. J. Wang *et al.*, Ligand-triggered allosteric ADP release primes a plant NLR complex. *Science* **364**, eaav5868 (2019).
12. G. Z. Bi *et al.*, The ZAR1 resistosome is a calcium-permeable channel triggering plant immune signaling. *Cell* **184**, 3528–3541.e12 (2021).
13. J. Wang *et al.*, Reconstitution and structure of a plant NLR resistosome conferring immunity. *Science* **364**, 1–11 (2019).
14. A. Forde *et al.*, A wheat resistosome defines common principles of immune receptor channels. *Nature* **610**, 532–539 (2022).
15. Y. B. Zhao *et al.*, Pathogen effector AvrSr35 triggers Sr35 resistosome assembly via a direct recognition mechanism. *Sci. Adv.* **8**, eabq5108 (2022).
16. S. Horsefield *et al.*, NAD(+) cleavage activity by animal and plant TIR domains in cell death pathways. *Science* **365**, 793–799 (2019).

17. S. Ma *et al.*, Direct pathogen-induced assembly of an NLR immune receptor complex to form a holoenzyme. *Science* **370**, 1–10 (2020).
18. R. Martin *et al.*, Structure of the activated ROQ1 resistosome directly recognizing the pathogen effector XopQ. *Science* **370**, 1–7 (2020).
19. S. Huang *et al.*, Identification and receptor mechanism of TIR-catalyzed small molecules in plant immunity. *Science* **377**, eabq3297 (2022).
20. A. Jia *et al.*, TIR-catalyzed ADP-ribosylation reactions produce signaling molecules for plant immunity. *Science* **377**, eabq8180 (2022).
21. L. Wan *et al.*, TIR domains of plant immune receptors are NAD(+)-cleaving enzymes that promote cell death. *Science* **365**, 799–803 (2019).
22. K. Essuman, J. Milbrandt, J. L. Dangl, M. T. Nishimura, Shared TIR enzymatic functions regulate cell death and immunity across the tree of life. *Science* **377**, eabo0001 (2022).
23. X. H. Sun *et al.*, Pathogen effector recognition-dependent association of NRG1 with EDS1 and SAG101 in TNL receptor immunity. *Nat. Commun.* **12**, 3335 (2021).
24. Z. S. Wu, L. Tian, X. R. Liu, Y. L. Zhang, X. Li, TIR signal promotes interactions between lipase-like proteins and ADR1-L1 receptor and ADR1-L1 oligomerization. *Plant Physiol.* **187**, 681–686 (2021).
25. Z. Gao, E. H. Chung, T. K. Eitas, J. L. Dangl, Plant intracellular innate immune receptor Resistance to *Pseudomonas syringae* pv. *maculicola* 1 (RPM1) is activated at, and functions on, the plasma membrane. *Proc. Natl. Acad. Sci. U.S.A.* **108**, 7619–7624 (2011).
26. D. Qi, B. J. DeYoung, R. W. Innes, Structure-function analysis of the coiled-coil and leucine-rich repeat domains of the RPS5 disease resistance protein. *Plant Physiol.* **158**, 1819–1832 (2012).
27. Y. Belkhadir, Z. Nimchuk, D. A. Hubert, D. Mackey, J. L. Dangl, Arabidopsis RIN4 negatively regulates disease resistance mediated by RPS2 and RPM1 downstream or independent of the NDR1 signal modulator and is not required for the virulence functions of bacterial type III effectors AvrRpt2 or AvrRpm1. *Plant Cell* **16**, 2822–2835 (2004).
28. M. Hu, J. Qi, G. Bi, J. M. Zhou, Bacterial effectors induce oligomerization of immune receptor ZAR1 in vivo. *Mol. Plant* **13**, 793–801 (2020).
29. S. C. Saile *et al.*, Arabidopsis ADR1 helper NLR immune receptors localize and function at the plasma membrane in a phospholipid dependent manner. *New Phytol.* **232**, 2440–2456 (2021).
30. C. Duggan *et al.*, Dynamic localization of a helper NLR at the plant-pathogen interface underpins pathogen recognition. *Proc. Natl. Acad. Sci. U.S.A.* **118**, e2104997118 (2021).
31. Z. S. Wu *et al.*, Differential regulation of TNL-mediated immune signaling by redundant helper CNLs. *New Phytol.* **222**, 938–953 (2019).
32. H. Adachi *et al.*, An atypical NLR protein modulates the NRC immune receptor network in *Nicotiana benthamiana*. *PLoS Genet.* **19**, e1010500 (2023).
33. H. Adachi *et al.*, An N-terminal motif in NLR immune receptors is functionally conserved across distantly related plant species. *Elife* **8**, e49956 (2019).
34. A. Schultink, T. Qi, A. Lee, A. D. Steinbrenner, B. Staskawicz, Roq1 mediates recognition of the *Xanthomonas* and *Pseudomonas* effector proteins XopQ and HopQ1. *Plant J.* **92**, 787–795 (2017).
35. S. Zhu *et al.*, SAG101 forms a ternary complex with EDS1 and PAD4 and is required for resistance signaling against turnip crinkle virus. *PLoS Pathog.* **7**, e1002318 (2011).
36. B. J. Feys *et al.*, Arabidopsis SENESCENCE-ASSOCIATED GENE101 stabilizes and signals within an ENHANCED DISEASE SUSCEPTIBILITY1 complex in plant innate immunity. *Plant Cell* **17**, 2601–2613 (2005).
37. J. Zonnchen *et al.*, EDS1 complexes are not required for PRR responses and execute TNL-ETI from the nucleus in *Nicotiana benthamiana*. *New Phytol.* **236**, 2249–2264 (2022).
38. M. Bernoux *et al.*, Subcellular localization requirements and specificities for plant immune receptor Toll-interleukin-1 receptor signaling. *Plant J.* **114**, 1319–1337 (2023), 10.1111/tpj.16195.
39. M. Bernoux *et al.*, Comparative analysis of the flax immune receptors L6 and L7 suggests an equilibrium-based switch activation model. *Plant Cell* **28**, 146–159 (2016).
40. V. Markovic, Y. Jaillais, Phosphatidylinositol 4-phosphate: A key determinant of plasma membrane identity and function in plants. *New Phytol.* **235**, 867–874 (2022).
41. Y. Dondelinger *et al.*, MLKL compromises plasma membrane integrity by binding to phosphatidylinositol phosphates. *Cell Rep.* **7**, 971–981 (2014).
42. Q. Chai *et al.*, A bacterial phospholipid phosphatase inhibits host pyroptosis by hijacking ubiquitin. *Science* **378**, eabq0132 (2022).
43. Y. Zhong, Z. M. Cheng, A unique RPW8-encoding class of genes that originated in early land plants and evolved through domain fission, fusion, and duplication. *Sci. Rep.* **6**, 32923 (2016).
44. D. C. Boyes, J. Nam, J. L. Dangl, The Arabidopsis thaliana RPM1 disease resistance gene product is a peripheral plasma membrane protein that is degraded coincident with the hypersensitive response. *Proc. Natl. Acad. Sci. U.S.A.* **95**, 15849–15854 (1998).
45. F. El Kasmi *et al.*, Signaling from the plasma-membrane localized plant immune receptor RPM1 requires self-association of the full-length protein. *Proc. Natl. Acad. Sci. U.S.A.* **114**, E7385–E7394 (2017).
46. B. P. M. Ngou, H. K. Ahn, P. T. Ding, J. D. G. Jones, Mutual potentiation of plant immunity by cell-surface and intracellular receptors. *Nature* **597**, 110–115 (2021), 10.1038/s41586-021-03315-7.
47. M. H. Yuan *et al.*, Pattern-recognition receptors are required for NLR-mediated plant immunity. *Nature* **592**, 105–109 (2021), 10.1038/s41586-021-03316-6.
48. R. N. Pruitt *et al.*, The EDS1-PAD4-ADR1 node mediates Arabidopsis pattern-triggered immunity. *Nature* **598**, 495–499 (2021).
49. Y. J. Li *et al.*, Plasma membrane-nucleo-cytoplasmic coordination of a receptor-like cytoplasmic kinase promotes EDS1-dependent plant immunity. *Nat. Plants* **8**, 802–816 (2022).
50. H. N. Tian *et al.*, Activation of TIR signalling boosts pattern-triggered immunity. *Nature* **598**, 500–503 (2021).
51. J. Kourelis *et al.*, The helper NLR immune protein NRC3 mediates the hypersensitive cell death caused by the cell-surface receptor Cf-4. *PLoS Genet.* **18**, e1010414 (2022).
52. H. K. Ahn *et al.*, Effector-dependent activation and oligomerization of plant NRC class helper NLRs by sensor NLR immune receptors Rpi-amr3 and Rpi-amr1. *EMBO J.* **42**, e11148 (2023), 10.15252/embj.2022111484.
53. M. P. Contreras *et al.*, Sensor NLR immune proteins activate oligomerization of their NRC helpers in response to plant pathogens. *EMBO J.* **42**, e111519 (2022), 10.15252/embj.2022111519.
54. J. M. Feehan *et al.*, Oligomerisation of a plant helper NLR requires cell-surface and intracellular immune receptor activation. *Proc. Natl. Acad. Sci. U.S.A.* **120**, e2210406120 (2023).
55. X. Liu *et al.*, RIN13-mediated disease resistance depends on the SNC1-EDS1/PAD4 signaling pathway in Arabidopsis. *J. Exp. Bot.* **71**, 7393–7404 (2020).
56. G. E. Crooks, G. Hon, J. M. Chandonia, S. E. Brenner, WebLogo: A sequence logo generator. *Genome Res.* **14**, 1188–1190 (2004).
57. F. W. Studier, Protein production by auto-induction in high density shaking cultures. *Protein Expr. Purif.* **41**, 207–234 (2005).
58. Y. Durocher *et al.*, Scalable serum-free production of recombinant adeno-associated virus type 2 by transfection of 293 suspension cells. *J. Virol. Methods* **144**, 32–40 (2007).